Quantum size effects on exciton states in indirect-gap quantum dots

D. H. Feng,[1] Z. Z. Xu,[1] T. Q. Jia,[1,2] X. X. Li,[1] and S. Q. Gong[1]
[1]*Laboratory for High Intensity Optics, Shanghai Institute of Optics and Fine Mechanics, Chinese Academy of Sciences, P. O. Box 800-211, Shanghai, 201800, China*
[2]*State Key Laboratory for Optical and Electric Materials and Technology, Zhongshan University, Guangzhou, 510275, China*
(Received 7 April 2003; published 30 July 2003)

We investigate exciton ground states in Si and 3C-SiC quantum dots by using the effective mass theory, taking account of the conduction- and valence-band mass anisotropy as well as the small spin-orbit splitting energy. The degenerate hole and exciton states are partly split by the mass anisotropy. The anisotropy splitting energies in quantum dots are different dramatically from their bulk value due to quantum size effects. The assumed changeable spin-orbit splitting energy may change the ordering of the anisotropy-split energy levels. Taking account of the exchange interaction, the degeneracy of the exciton states is further lifted. Due to the anisotropy and exchange splitting, the 48-fold exciton ground state will be split into two 18-fold triplets and two 6-fold singlets. The lowest three states are optically forbidden for Si quantum dots, which leads to a Stokes shift of luminescence. The theroretical shift agrees well with the experimental data. Furthermore, the exciton band gap and binding energy as a function of dot radius are presented both for Si and for 3C-SiC quantum dots. The band gap of Si quantum dots agrees well with the recent photoluminescence results of size-separated quantum dots by Ledoux *et al.* and absorption data of Furukawa *et al.*

DOI: 10.1103/PhysRevB.68.035334 PACS number(s): 73.20.Mf, 71.35.Cc, 73.21.La

I. INTRODUCTION

Recently zero-dimensional quantum dots (QD's) have attracted much attention not only for a variety of new interesting physical and chemical properties but also for their potential applications.[1,2] Many experimental and theoretical investigations have focused on quantum size effects. When their size approaches the exciton Bohr radius, QD's exhibit new properties that differ dramatically from those of the bulk material. One case of quantum size effects is the tunable band gap as a function of quantum size. In addition, many indistinctive properties in bulk materials may be enhanced considerably in QD's. For example, the exchange splitting energy can be increased by 3 orders of magnitude as the size of semicondutors is reduced from bulk to nanoscale.[3]

The strong visible luminescence in porous silicon[4] stirred up an intensive investigation of its origin. Although the emission mechanism is still under debate, the quantum confinement in Si QD's is mostly accepted as the main explanation. While many experimental phenomena can be explained in terms of quantum confinement, arriving at a quantitative agreement between theory and experiment is still extremely challenging.[5] Recently photoluminescence experiments of size-separated QD's have been performed by Ledoux *et al.*[6] The exciton band gap of size-separated QD's is larger than photoluminescence (PL) results of porous Si.[7] Many calculated exciton gaps, including the recent tight-binding theoretical data of Lee *et al.*[8] and pseudopotential calculation results of Reboredo *et al.*,[9] are lower than the gap of size-separated QD's. Takagahara and Takeda[10] calculated the exciton energy and binding energy of Si QD's using four-band effective mass theory (EMT). They clarified a mechanism which induces an indirect-to-direct conversion of the character of the optical transition. However, the Hamiltonian model in their calculation was not sufficiently accurate (e.g., a 4×4 Hamiltonian is not proper for QD's with a small spin-orbit splitting energy and effects of the strong band anisotropy were not taken into account), and the calculated result cannot be expected to be quantitatively correct.

EMT can naturally take account of the mass anisotropy both in the conduction and in the valence band. The mass anisotropy has a significant effect on the fine structure of exciton states. In direct-gap cubic semiconductor quantum dots, the exciton ground state is eightfold in a spherical model. Differing from direct-gap semiconductors, the conduction-band minimum in Si is along the $\Delta=(0,0,k)$ direction, which has six equivalent points. The electron in Si has a strong mass anisotropy which leads to a splitting of the degenerate 48-fold exciton ground state partly. On the other hand, the valence-band anisotropy is also strong because the Luttinger parameters are largely different ($\gamma_1=4.10$, $\gamma_2=0.44$, $\gamma_3=1.40$). The spherical model ($\gamma_2=\gamma_3$, which is usually used for direct-gap QD's) is not proper anymore. The considerable difference in valence bands will partly lift the degeneracy of hole and exciton states. Although the mass anisotropy splitting in bulk Si has been intensively investigated,[11–13] to our knowledge, no work concerns this splitting in Si QD's which is expected to differ from that in bulk material due to quantum size effects.

The fine structure resulting from electron-hole exchange interactions has been intensively investigated.[3,14] The exchange splitting may result in ''dark'' and ''bright'' excitons, which leads to a Stokes shift in the luminescence. However, the effects of the mass anisotropy on exciton dark-bright properties are lacking an investigation and are unknown.

We use EMT to investigate these problems, taking account of the mass anisotropy and small spin-orbit splitting energy. Due to taking the mass anisotropy into account, not only the exciton energy but also effects of mass anisotropy on the fine structure and optical properties can be investigated.

As another important semicondutor, SiC is a promising

wide-band-gap material because of its superior characteristics such as high breakdown field strength, high thermal conductivity, and high saturation drift velocity.[15] Low-dimensional SiC has been intensively investigated experimentally. Many photoluminescence experiments show that a blueshift emission peak existing in porous 3C-SiC (Ref. 16) and in encapsulated nanoparticles.[17] Those transitions above the bulk band gap have been explained by the quantum confinement effect. Few theoretical investigations have been done, however, on the exciton states in SiC QD's which play an important role in interpreting the origin of the blueshift. Due to the similar band anisotropy to Si and the small spin-orbit splitting energy, we can easily treat the exciton states in 3C-SiC QD's following the route of Si QD's.

In this paper, we investigate the quantum size effects on the exciton states in Si and 3C-SiC QD's by using EMT. We lay emphasis on the anisotropy splitting, electron-hole exchange interaction, exciton band gap, and binding energy. For Si QD's, it is found that EMT can present a theroretical exciton band gap agreeing well with recent photoluminescence results of size-separated QD's. Taking account of both the mass anisotropy and exchange interaction, a larger bright-dark exciton splitting can be obtained than by only taking exchange splitting into account and agree well with experimental results. This article comprises the following. First we will present the calculation method. Then, our numerical results will be discussed and compared with the experimental data. Finally, a brief conclusion is drawn in our investigation.

II. CALCULATION METHOD

A. Confinement for electron states

In order to simplify the analysis, we only consider QD's as spheres with radius a surrounded by an infinitely high potential barrier. This model can be used in the treatment of porous Si (and SiC) and single nanoparticles.

The conduction-band minimum is located at $2\pi/a(0,0,0.85)$ and $2\pi/a(0,0,1)$ for Si and 3C-SiC, respectively. The effective mass at the conduction-band bottom is anisotropic and has an axial symmetry in the k_0 direction, which will be referred as the z directon. The effective mass Hamiltonian can be written as

$$H_e=\frac{1}{2m_\perp}(p_1^2+p_2^2)+\frac{1}{2m_\parallel}(p_3^2), \tag{1}$$

where $m_\perp$, $m_\parallel$ are the effective mass in the conduction bands perpendicular to and parallel to the z axis, respectively, 1, 2, 3 label the principal directions of a conduction-band ellipsoid. Equation (1) can be rewritten as

$$H_e=\frac{p_e^2}{2m_a}-\frac{1}{2m_b}\sqrt{\frac{2}{3}}P_0^{(2)}, \tag{2}$$

where $P_0^{(2)}$ is the second-order tensor of the momentum operator, which represents the anisotropy of the conduction-band minima. m_a, m_b are defined as

$$\frac{1}{m_a}=\frac{1}{3}\left(\frac{2}{m_\perp}+\frac{1}{m_\parallel}\right),$$
$$\frac{1}{m_b}=\frac{1}{3}\left(\frac{1}{m_\perp}-\frac{1}{m_\parallel}\right). \tag{3}$$

Due to the anisotropy term $P_0^{(2)}$, the angular momentum of the electronic states is no longer a good quantum number. Because of the axial symmetry, the z component of the total angular momentum of the electronic state remains a good quantum number. The lowest state $1S_e$ can be given as

$$\Psi_e=g_1(r_e)|00\rangle+g_2(r_e)|20\rangle+g_3(r_e)|40\rangle+\cdots, \tag{4}$$

where $|lm\rangle$ is the spherical harmonic function Y_{lm}; the parity of each state is a good quantum number. The radial wave functions $g_i(r_e)$ can be expanded using spherical Bessel functions

$$g_i(r_e)=\sqrt{\frac{2}{a^3}}\sum_{n=1}^{\infty}c_{nl}\frac{j_l(\alpha_{nl}\ r_e/a)}{j_{l+1}(\alpha_{nl})}, \tag{5}$$

where α_{nl} is the nth root of the spherical Bessel function $j_l(r_e=a)=0$.

In the calculation of the matrix element we will use a key equation

$$\langle l'\ m'|P_q^{(2)}|lm\rangle=\langle\ l,m;2,q\ |l',m'\rangle\frac{1}{\sqrt{2l'+1}}(l'\|P^{(2)}\|l), \tag{6}$$

where $\langle\ l,m;2,q\ |l',m'\rangle$ is the Clebsch-Gordan coefficient and $(l'\|P^{(2)}\|l)$ is the reduced matrix elements of the second-order momentum tensor, which are not zero only for $l'=l$ or $l'=l\pm2$. The detailed expressions of $(l'\|P^{(2)}\|l)$ are given in Ref. 18.

B. Confinement for hole states

Taking account of the anisotropy in the valence-band and spin-orbital coupling, the effective mass Hamiltonian in the hole states with an axial model can be written as[11,12]

$$H_h=\frac{\gamma_1}{2m_0}\left\{P_h^2-\frac{\mu}{3}[P^{(2)}\cdot I^{(2)}]+\frac{\sqrt{70}}{15}\sigma[P^{(2)}\times I^{(2)}]_0^4+\frac{2}{3}\left(\frac{1}{2}-I\cdot S\right)\Delta_{so}\right\}, \tag{7}$$

where γ_1, γ_2, γ_3 are Luttinger parameters, $\mu=(6\gamma_3+4\gamma_2)/5\gamma_1$, $\sigma=(\gamma_3-\gamma_2)/\gamma_1$, m_0 is the free-electron mass, I is the angular momentum operator corrsponding to spin 1, and S is the spin 1/2 of the hole. Δ_{so} is the valence-band spin-orbit splitting energy. The definitions for the tensor operators $P^{(2)}$, $I^{(2)}$ and their products were given in Ref. 18.

The wave functions for the above Hamiltonian can be written as

$$\Psi_h=\sum_i\ f_i(r_h)|L_i,J_i,F_i,F_{zi}\rangle, \tag{8}$$

$$|L,J;F,F_z\rangle=\sum_{L_z,J_z}\langle L,L_z;J,J_z|F,F_z\rangle|L,L_z\rangle|J,J_z\rangle. \quad (9)$$

Like $g_i(r_e)$ for electron states, the radial wave functions $f_i(r_h)$ can be expanded using spherical Bessel functions. The function $|L,J;F,F_z\rangle$ is an eigenfunction of the total angular momentum in the L-J coupling scheme; L,J,F,F_z are the quantum numbers of the envelope angular momentum, the Bloch angular momentum of the valence-band top, the total angular momentum, and the component of the total angular momentum along the z direction, respectively. $|L,L_z\rangle$ is the spherical harmonic function Y_{LL_z}, $|J,J_z\rangle$ is the Bloch wave funtion, and J can be assumed the values $\frac{3}{2}$ and $\frac{1}{2}$ which corresponds to the main (heavy and light) and split-off states, repectively. $\langle L,L_z;\ J,J_z|F,F_z\rangle$ is the Clebsch-Gordan coefficient. If taking a spherical approximation, F,F_z are considered as a good quantum number. While in the axial model taking anisotropy into account, F is not a good quantum number, although F_z remains its conservation. The wave function expansion would include an infinite number of L, which is truncated into a finite number of L in the calculation.

The matrix element with respect to the basis set can be written as

$$\begin{aligned}\langle L',J',F',F_z'|(P^{(2)}\cdot I^{(2)})|L,J,F,F_z\rangle&\\ =(-1)^{L+J'+F}\begin{Bmatrix}F & J' & L'\\ 2 & L & J\end{Bmatrix}(J'\|I^{(2)}\|J)&\\ \times(L'\|P^{(2)}\|L)\,\delta_{F',F}\delta_{F_z',F_z},&\end{aligned} \quad (10)$$

$$\begin{aligned}\langle L',J',F',F_z'|[P^{(2)}\times I^{(2)}]^4_m|L,J,F,F_z\rangle&\\ =3(-1)^{F'-F_z'}\sqrt{(2F'+1)(2F+1)}\begin{pmatrix}F' & 4 & F\\ -F_z' & m & F_z\end{pmatrix}&\\ \times\begin{pmatrix}J' & J & 2\\ L' & L & 2\\ F' & F & 4\end{pmatrix}(J'\|I^{(2)}\|J)(L'\|P^{(2)}\|L),&\end{aligned} \quad (11)$$

where

$$\begin{aligned}((IS)J'\|I^{(2)}\|(IS)J)=(-1)^{I+S+J+2}\sqrt{(2J'+1)(2J+1)}&\\ \times\begin{Bmatrix}I & J' & S\\ J & I & 2\end{Bmatrix}(I\|I^{(2)}\|I).&\end{aligned} \quad (12)$$

These matrix elements are expressed in terms of $3j$, $6j$, $9j$ symbols and the reduced matrix elements $(L'\|P^{(2)}\|L)$ and $(I\|I^{(2)}\|I)$. The detailed information of nj symbols can be found in Ref. 19. The calculation expressions of the reduced matrix elements of the second-order momentum tensor are given in Ref. 18.

C. Confinement for exciton states

The exciton Hamiltonian in a quantum sphere is given by

$$H_{ex}=H_e+H_h-\frac{e^2}{\epsilon r_{eh}}, \quad (13)$$

where ϵ is the dielectric constant and $r_{eh}=|r_e-r_h|$. The exciton wave function can be expanded in terms of electron and hole functions as

$$\Psi_{ex}(r_e,r_h)=\sum_{i,j}c_{ij}\Psi_{ei}(r_e)\Psi_{hj}(r_h), \quad (14)$$

where $\Psi_{ei}(r_e)$ and $\Psi_{hj}(r_h)$ are the wave functions of electronic and hole eigenstates, respectively. In the calculations of the Coulomb interaction,

$$\frac{1}{r_{eh}}=\sum_{k=0}^{\infty}\frac{r_<^k}{r_>^{k+1}}P_k(\cos\theta_{eh}), \quad (15)$$

$$P_k(\cos\theta_{eh})=\frac{4\pi}{2k+1}\sum_{m=-k}^{k}Y^*_{km}(\theta_e,\varphi_e)Y_{km}(\theta_h,\varphi_h), \quad (16)$$

where $r_>=\max(r_e,r_h)$, $r_<=\min(r_e,r_h)$, P_k are the Legendre polynomials, and θ_{eh} is the angle between the position vectors of electron (r_e) and hole (r_h).

In the calculation of the matrix element of the Coulomb interaction, the following equations will be used:

$$Y^*_{km}=(-1)^mY_{k-m}, \quad (17)$$

$$\begin{aligned}\langle l_e',m_e'|Y_{k-m}|l_e,m_e\rangle=\sqrt{\frac{(2l+1)(2k+1)}{4\pi(2l'+1)}}\langle l,0;k,0|l',0\rangle&\\ \times\langle l_e,m_e;k,-m|l_e',m_e'\rangle,&\end{aligned} \quad (18)$$

$$\begin{aligned}\langle L',J',F',F_z'|Y_{km}|L,J,F,F_z\rangle&\\ =\langle F,F_z;k,m|F',F_z'\rangle\frac{1}{\sqrt{2F'+1}}\langle L',J',F'\|Y_k\|L,J,F\rangle,&\end{aligned} \quad (19)$$

where

$$\begin{aligned}\langle L',J',F'\|Y_k\|L,J,F\rangle&\\ =(-1)^{(L'+J+F+k)}\sqrt{(2F+1)(2F'+1)}&\\ \times\begin{Bmatrix}L' & L & k\\ F & F' & J'\end{Bmatrix}\langle L'\|Y_k\|L\rangle\,\delta_{JJ'},&\end{aligned} \quad (20)$$

and

TABLE I. Material parameters used in our calculations. E_g is the bulk band gap. $m_\perp$, $m_\parallel$ are the effective mass in the conduction band perpendicular to and parallel to the z axis. $\gamma_1, \gamma_2, \gamma_3$ are Luttinger parameters. Δ_{so} is the spin-orbit splitting energy.

	E_g(eV)	$m_\perp$	$m_\parallel$	γ_1	γ_2	γ_3	Δ_{so}(meV)
Si	1.17[a]	0.30,[b] 0.19[a]	0.91,[b] 0.92[a]	4.10[c]	0.44[c]	1.40[c]	44.1[a]
SiC	2.39[a]	0.25[a]	0.67[a]	1.820[d]	0.155[d]	0.648[d]	14.5[a]

[a]Reference 20.
[b]Reference 8.
[c]Reference 21.
[d]Reference 22.

$$\langle\ L'\|Y_k\|L\rangle = \sqrt{\frac{(2L+1)(2k+1)}{4\pi}}\langle L,0;k,0|L',0\rangle. \tag{21}$$

III. RESULTS AND DISCUSSION

Table I lists the parameters used in our calculations. Here we adopt different electron effective masses for different size regions, experimental data $m_\perp=0.19$, $m_\parallel=0.92$ for dot radius $a>2$ nm, and recent calculational data $m_\perp=0.30$, $m_\parallel=0.91$ for dot radius $a<2$ nm. Calculations for Si QD's (see below)show that, with $m_\perp=0.19$, $m_\parallel=0.92$, theoretical results agree well with experiments for dot radius $a>2$ nm, but yield overestimated numerical results for $a<2$ nm. Taking account of the fact that the surface effects in very small dots may bring on a change of effective masses which differs from bulk value,[23,24] we take the effective mass of electrons $m_\perp=0.30$, $m_\parallel=0.91$ for dot radius $a<2$ nm, which are calculated with optimized tight-binding parameters.[8] The tranverse effective mass $m_\perp=0.30$ is slightly larger than the bulk data $m_\perp=0.19$, but this value approaches the calculated result[23] in 2 nm wire thickness using a first-principles pseudopotential method.

The dielectric constant in Eq. (13) is the static dielectric constant. Compared with the bulk value, this constant will become small as the dot radius decreases due to the quantum confinement. For Si, the size-dependent dielectric constant in the parameter form was presented in Ref. 25. We will follow this procedure in the calculation below. For SiC, due to the lack of a similar function, taking account of the fact that the binding energy exceeds the optical phonon energy, we will adopt the high-frequency value of the dielectric function[26] $\epsilon_\infty=6.52$ for a dot radius smaller than 2.0 nm and the static value $\epsilon_0=9.72$ for sizes larger than 2.0 nm as an approximation.

Figure 1 shows the anisotropy splittings of the hole and exciton ground states versus dot radius. As the dot radius decreases, an obvious change in the splitting energy takes place due to quantum size effects. As we can see, the change tendency in Si QD's is largely different from the case for 3C-SiC QD's. For Si QD's, in the investigated range of dot radius, both hole and exciton splitting increase with radius decreasing. As the dot radius is reduced to 1 nm, the exciton ground splitting can be enhanced to about 14 meV, which is much larger than the corresponding bulk value 0.32 meV.[12] Compared with Si, the hole and exciton splitting energies in 3C-SiC QD's increase very slightly at first and then decrease. When the splitting value is lower than zero, it means $1S_{3/2}^{\pm 1/2}$ (here we use the main component $nL_F^{F_z}$ for notation) becomes the lowest states. This case is different from bulk SiC not only in the splitting value but in the level ordering. Further calculations show that the small Δ_{so} in 3C-SiC mainly accounts for this difference. Figure 2 presents a straightforward illustration. Given a larger spin-orbit splitting energy (e.g., 44 meV which equals that in Si), the split hole level ordering can change, differing from the case of $\Delta_{so}=14.5$ meV. Oppositely, with $\Delta_{so}=0$ meV, a magnitude of $1S_{3/2}^{\pm 1/2}$ lower than $1S_{3/2}^{\pm 3/2}$ would become larger than that in the case of $\Delta_{so}=14.5$ meV. A smaller spin-orbit splitting

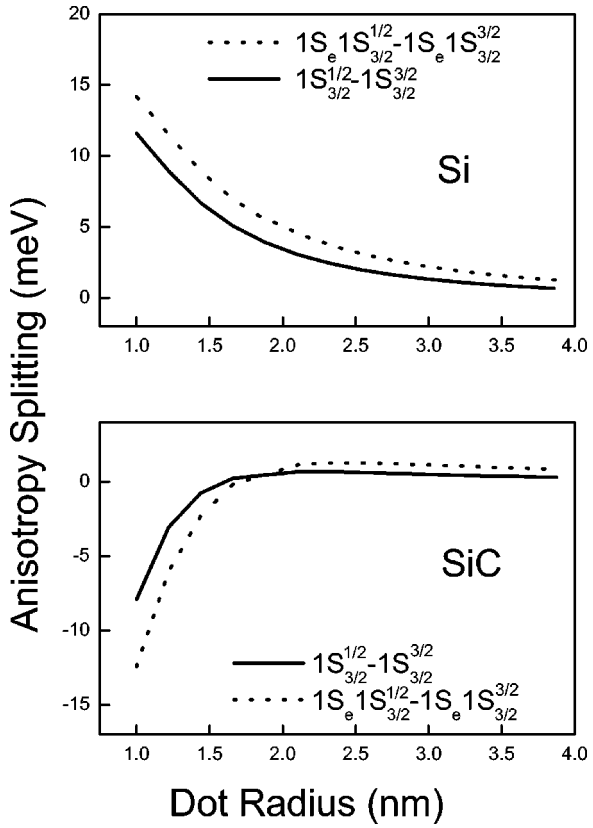

FIG. 1. The anisotropy splitting energy for hole ($1S_{3/2}^{\pm 1/2}$-$1S_{3/2}^{\pm 3/2}$) and exciton ($1S_e1S_{3/2}^{\pm 1/2}$-$1S_e1S_{3/2}^{\pm 3/2}$) ground states as a function of dot radius for Si and 3C-SiC quantum dots.

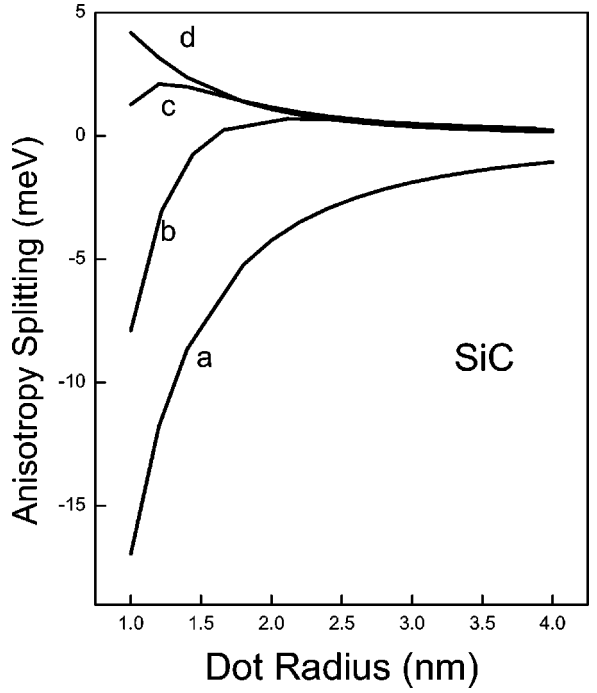

FIG. 2. The anisotropy splitting energy for hole ground states of 3C-SiC quantum dots ($1S_{3/2}^{\pm 1/2}$-$1S_{3/2}^{\pm 3/2}$) as a function of dot radius, with an assumed changeable spin-orbit splitting energy Δ_{so}. *a*, *b*, *c*, and *d* correspond to $\Delta_{so}=0$, 14.5, 44, and 100 meV, respectively. The changed Δ_{so} may give a changed level ordering between $1S_{3/2}^{\pm 1/2}$ and $1S_{3/2}^{\pm 3/2}$.

energy means a stronger coupling between the main (heavy and light) and split-off states. When the spin-orbit splitting energy is large, the level ordering is affected mainly by the mass anisotropy. While the spin-orbit splitting energy is small, the level ordering is affected both by the mass anisotropy and by the coupling between different states. Consequently, the magnitude of spin-orbit splitting is important for the fine structure in QD's.

For Si QD's, the lowest hole state is $1S_{3/2}^{\pm 3/2}$; a thermalization of the holes initially excited into higher states can lead to the formation of long-lived $|1S_{3/2}^{3/2},1S_e(\downarrow)\rangle$ and $|1S_{3/2}^{-3/2},1S_e(\uparrow)\rangle$ electron-hole pair states.[27] Taking account of the electron-hole exchange interaction, the 24-fold exciton states $1S_e1S_{3/2}^{\pm 3/2}$ and $1S_e1S_{3/2}^{\pm 1/2}$ will be further split. Figure 3 shows a schematic representation of the anisotropy splitting and further exchange splitting. The lowest exchange-split state is a pure triplet and spin forbidden (''dark''). Although the singlet state split from $1S_e1S_{3/2}^{\pm 3/2}$ is spin allowed, it is spatially forbidden (''dark''), as its wave function is a combination of the long-lived $|1S_{3/2}^{3/2},1S_e(\downarrow)\rangle$ and $|1S_{3/2}^{-3/2},1S_e(\uparrow)\rangle$ states. Only the singlet state in $1S_e1S_{3/2}^{\pm 1/2}$ is optically allowed (''bright''). The formation of the transition-forbidden lowest states can lead to a Stokes shift of luminescence. The shift equals an exchange energy of $1S_e1S_{3/2}^{\pm 1/2}$ plus the anisotropy splitting energy between $1S_e1S_{3/2}^{\pm 1/2}$ and $1S_e1S_{3/2}^{\pm 3/2}$ states. Calculation of the exact exchange energy is much more complicated, since the exchange energy includes two parts of the short-range and long-range interactions. As an approximation, we consider only the short-range part which can be expressed as[14,29] $E_{exch}(r)=\pi\alpha_{ex}^3 J\int dr|\Psi_{ex}(r,r)|^2$, where J is the exchange energy of the $1s$ bulk exciton, $J=0.15$ meV (Ref. 13) for Si, α_{ex} is the Bohr radius of the $1s$ bulk exciton, and $\alpha_{ex}=0.43$ nm.[11] When both the mass anisotropy and exchange interactions are taken into account, the bright-

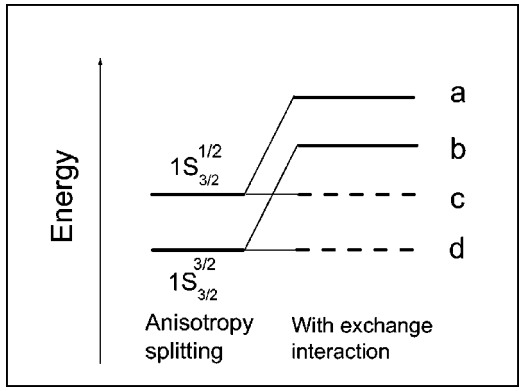

FIG. 3. A schematic representation of the anisotropy splitting and further exchange splitting. The dashed lines are pure triplets (line *c* and line *d*) which are spin forbidden (''dark'' exciton). The singlet (line *b*) in $1S_e1S_{3/2}^{\pm 3/2}$ is spatially forbidden (''dark'' exciton). Only the singlet (line *a*) is optically allowed (''bright'' exciton).

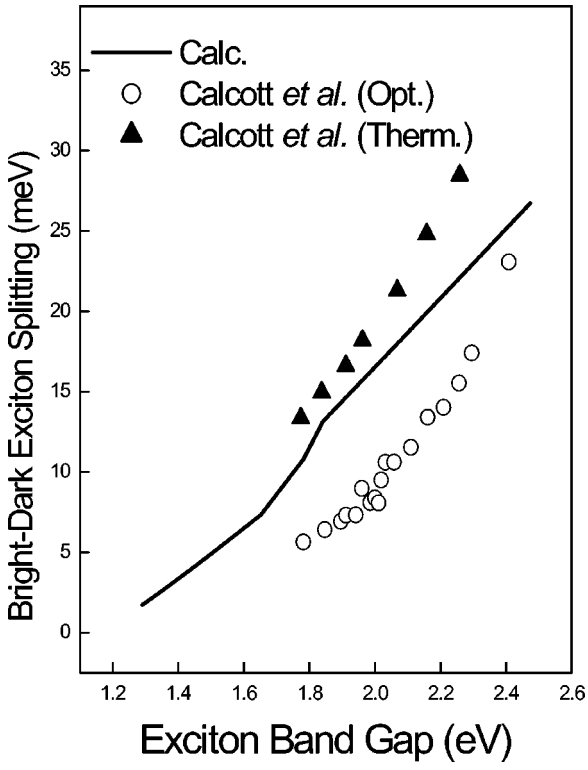

FIG. 4. Energy splitting between the lowest bright state and the lowest dark state as a function of the dark exciton energy. The solid line corresponds to the present calculations; the experimental data are taken from the optical onset measurements and thermal PL decay measurements results of Calcott *et al.* (Ref. 30).

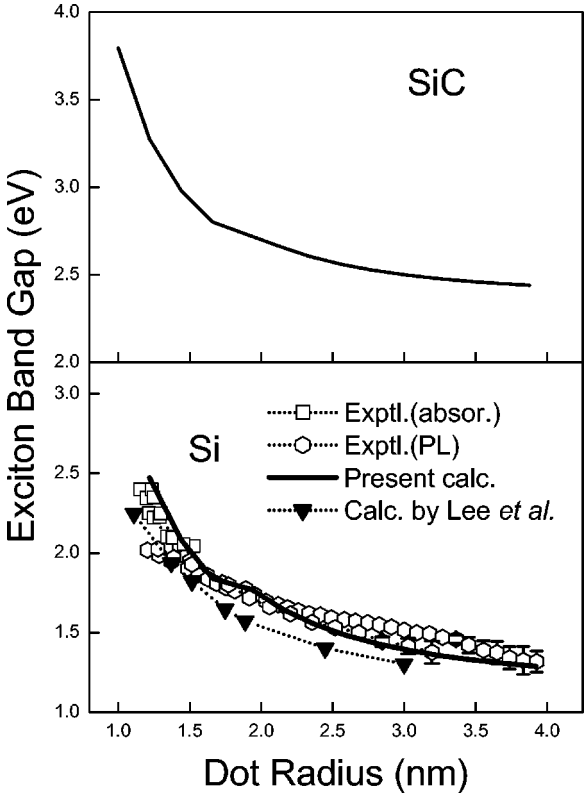

FIG. 5. Exciton band gap vs dot radius for Si and 3C-SiC quantum dots. The photoluminescence experimental data are taken from the recent results of size-separated quantum dots by Ledoux *et al.* (Ref. 6). The absorption experimental data are taken from Ref. 28. The other set of exciton gap are calculated by Lee *et al.* (Ref. 8) using tight-binding theory. We adopt the effective mass calculated by Lee *et al.* (Ref. 8) with optimized tight-binding parameters for dot radius $a<2$ nm, and experimental effective mass data for $a>2$ nm. The present calculations give better agreement with size-separated experiments than the calculation by Lee *et al.*

dark exciton splitting energy is larger than that in the case of only taking account of exchange splitting. The calculated bright-dark exciton splitting as a function of dot radius is plotted in Fig. 4 and agrees well with the optical onset measurements and thermal PL decay measurements results of Calcott *et al.*[30]

Figure 5 presents the calculated exciton band gap as a function of the dot radius for both Si and 3C-SiC. For 3C-SiC, because of a lack of detailed experimental or theoretical data, only present calculation results are given. For Si, the recent experimental data by Ledoux *et al.*[6] and by Furukawa and Miyasato,[28] as well as the theoretical value by using tight-binding method[8] are also shown as a comparison. In the experiment by Ledoux *et al.*,[6] the silicon nanocrystal samples were prepared by pulsed CO_2 laser pyrolysis of silane in a gas-flow reactor and expanded through a conical nozzle into a high vacuum. Using a fast-spinning molecular-beam chopper, they were size selectively deposited on dedicated quartz substrates. Due to a narrow size distribution, their PL emission lies slightly below the absorption experiment. Although Lee *et al.*[8] gave a result agreeing well with photoluminescence experimental data by Wolkin *et al.*[7] in

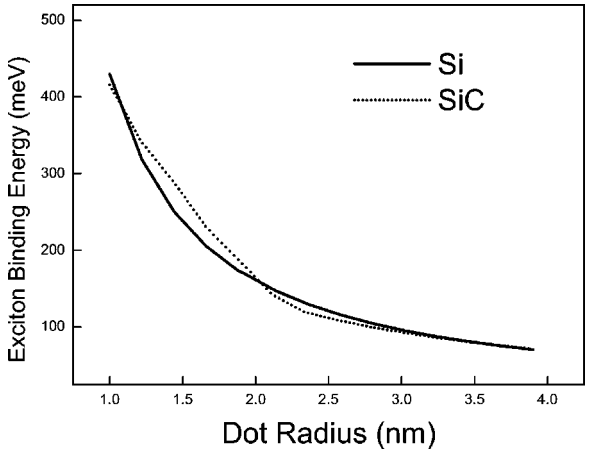

FIG. 6. Exciton binding energy vs dot radius for Si and 3C-SiC quantum dots.

their tight-binding calculations, their results have a considerable discrepancy compared with the size-separated photoluminesence data. Note that, due to a board size distribution on porous Si, the experimental results for porous Si may be less reliable than the size-separated results. If we use the effective mass calculated with the optimized tight-binding parameters of Lee *et al.* for dot radius $a<2$ nm, however, a better result can be obtained. For the overall size region in our investigation, with the parameters in Table I, the numerical results (shown in Fig. 5) are in a fairly good agreement with absorption and size-selective photoluminescence experiments.

The exciton binding energies both for Si and SiC QD's are shown in Fig. 6 as a function of dot radius. Comparing to their bulk value (14.3 meV for Si and 26.7 meV for 3C-SiC), the binding energies increase largely in QD's. It is because of the quantum confinement and a lower dielectric constants in QD's. Because of the strong binding in an electron-hole pair, stable exciton states exist even at room temperature, while bulk exciton states usually exist only at low temperture.

IV. CONCLUSION

In this paper, we investigated quantum size effects on Si and 3C-SiC QD's using a strict effective mass Hamiltonian, taking the band mass anisotropy and the small spin-orbit splitting energy into account. First, we studied the anisotropy splitting both in Si and in 3C-SiC QDs. Due to the conduction- and valence-band mass anisotropy, the degenerate hole and exciton states are partly split. For Si QD's, the exciton anisotropy splitting energies (with $1S_e1S_{3/2}^{\pm 3/2}$ lower than $1S_e1S_{3/2}^{\pm 1/2}$) increase largely as the dot radius decreases while in the case of 3C-SiC QD's the ordering between $1S_e1S_{3/2}^{\pm 1/2}$ and $1S_e1S_{3/2}^{\pm 3/2}$ can change in different size regions. Taking account of the exchange interaction, the degenerate exciton states are further lifted. For Si QD's, the 48-fold exciton ground state will be split into two 18-fold triplets and two 6-fold singlets with mass anisotropy and electron-hole interactions. The lowest three exciton states are

optically forbidden. They lead to a Stokes shift of the luminescence. The theoretical Stokes shift agrees well with the experimental data. Then, we presented the numerical exciton band gap and binding energies as a function of dot radius both for Si and 3C-SiC quantum dots. The exciton band gap in Si QD's is in good agreement with the recent size-separated photoluminescence and absorption experiments.

ACKNOWLEDGMENTS

This work was supported by the Chinese National Major Basic Research Project under Grant No. G1999075200 and Chinese National Natural Science Foundation under Grant No. 60108002. The authors thank Professor Junjie Shi and Dr. Jingbo Li for helpful discussions.

[1] V. I. Klimov, A. A. Mikhailovsky, Su Xu, A. Malko, J. A. Hollingsworth, C. A. Leatherdale, H.-J. Eisler, and M. G. Bawendi, Science **290**, 314 (2000).
[2] C. J. Wang, M. Shim, and P. Guyot-Sinonnest, Science **291**, 2390 (2001).
[3] T. Takagahara and K. Takeda, Phys. Rev. B **53**, R4205 (1996).
[4] L. T. Canham, Appl. Phys. Lett. **57**, 1046 (1990).
[5] A. G. Cullis, L. T. Canham, and P. D. J. Calcott, J. Appl. Phys. **82**, 909 (1997).
[6] G. Ledoux, J. Gong, F. Huisken, O. Guillois, and C. Reynaud, Appl. Phys. Lett. **80**, 4834 (2002).
[7] M. V. Wolkin, J. Jorne, P. M. Fauchet, G. Allan, and C. Delerue, Phys. Rev. Lett. **82**, 197 (1999).
[8] S. Lee, L. Jonsson, J. W. Wilkins, G. W. Bryant, and G. Klimeck, Phys. Rev. B **63**, 195318 (2001).
[9] F. A. Reboredo, A. Franceschetti, and A. Zunger, Phys. Rev. B **61**, 13073 (2000); Appl. Phys. Lett. **75**, 2972 (1999).
[10] T. Takagahara and K. Takeda, Phys. Rev. B **46**, 15 578 (1992).
[11] N. O. Lipari and M. Altarelli, Phys. Rev. B **15**, 4883 (1977); M. Altarelli and N. O. Lipari, *ibid.* **15**, 4898 (1977).
[12] N. O. Lipari and M. Altarelli, Solid State Commun. **32**, 171 (1979).
[13] J. C. Merle, M. Capizzi, P. Fiorini, and A. Frova, Phys. Rev. B **17**, 4821 (1978).
[14] J. M. Ferreyra and C. R. Proetto, Phys. Rev. B **60**, 10 672 (1999).
[15] M. Bhatnagar and B. J. Baliga, IEEE Trans. Electron Devices **40**, 645 (1993).
[16] L. S. Liao, X. M. Bao, Z. F. Yang, and N. B Min, Appl. Phys. Lett. **66**, 2382 (1995).
[17] X. Li, C. Shao, S. Qiu, F. S. Xiao, W. Zheng, Z. Liu, and O. Terasaki, Mater. Lett. **48**, 242 (2001).
[18] A. Baldereschi and N. O. Lipari, Phys. Rev. B **8**, 2697 (1973).
[19] A. R. Edmonds, *Angular Momentum in Quantum Mechanics* (Princeton University Press, Princeton, 1974).
[20] C. Persson and U. Lindefelt, Phys. Rev. B **54**, 10 257 (1996).
[21] J. R. Chelikowski and M. L. Cohen, Phys. Rev. B **10**, 5095 (1974).
[22] M. Willatzen, M. Cartona, and N. E. Christensen, Phys. Rev. B **51**, 13 150 (1995).
[23] R. J. Needs, S. Bhattacharjee, K. J. Nash, A. Qteish, A. J. Read, and L. A. Canham, Phys. Rev. B **50**, 14 223 (1994).
[24] E. Vázquez, J. Tagüeña-Martínez, L. E. Sansores, and C. Wang, J. Appl. Phys. **91**, 3085 (2002).
[25] S. Ögüt, J. R. Chelikowsky, and S. G. Louie, Phys. Rev. Lett. **79**, 1770 (1997).
[26] D. Bimberg, M. Altarelli, and N. O. Lipari, Solid State Commun. **40**, 437 (1981).
[27] Al. L. Efros and A. V. Rodina, Phys. Rev. B **47**, 10 005 (1993).
[28] S. Furukawa and T. Miyasato, Phys. Rev. B **38**, 5726 (1988).
[29] T. Takagahara, Phys. Rev. B **47**, 4569 (1993).
[30] P. D. J. Calcott, K. J. Nash, L. T. Canham, M. J. Kane, and D. Brumhead, J. Phys.: Condens. Matter **5**, L91 (1993).